visual analysis of FDG PET images in pulmonary abnormalities. *J Nucl Med* 1994;35:1771–1776.
39. Mori K, Yokoi K, Saito Y, Tominaga K, Miyazawa N. Diagnosis of mediastinal lymph node metastases in lung cancer. *Jpn J Clin Oncol* 1992;22:35–40.
40. Keyes JW. SUV: standard uptake or silly useless value? *J Nucl Med* 1995;36:1836–1839.
41. Tonami N, Yokoyama K, Shuke N, et al. Evaluation of suspected malignant pulmonary lesions with ^{201}Tl single-photon emission computed tomography. *Nucl Med Commun* 1993;14:602–610.
42. Suga K, Kume N, Orihashi, N, et al. Difference in ^{201}Tl accumulation on single photon emission computed tomography in benign and malignant thoracic lesions. *Nucl Med Commun* 1993;14:1071–1078.
43. Orihashi N, Mita T, Uchisaka H, Suga K, Matsumoto T, Nakanishi T. Tl-201 SPECT in the evaluation of small nodular lesions of lung. *Jap J Clin Radiol* 1994;39:159–163.
44. Martin WH, Delbeke D, Patton JA, Sandler MP. Detection of malignancies with SPECT versus PET, with 2-[Fluorine-18]fluoro-2-deoxy-D-glucose. *Radiology* 1996; 198:225–231.
45. Drane WE, Abbott FD, Nicole MW, Mastin ST, Kuperus JH. Technology for FDG SPECT with a relatively inexpensive gamma camera. *Radiology* 1994;191:461–465.
46. Macfarlane DJ, Cotton L, Ackermann RJ, et al. Triple-head SPECT with 2-[fluorine-18] fluoro-2-deoxy-D-glucose (FDG): initial evaluation in oncology and comparison with FDG PET. *Radiology* 1995;194:425–429.
47. Slosman DO, Pugin J. Lack of correlation between tritiated deoxyglucose, thallium-201 and technetium-99m-MIBI cell incorporation under various cell stresses. *J Nucl Med* 1994;35:120–126.
48. Kubota R, Kubota K, Yamada S, et al. Active and passive mechanisms of [fluorine-18]fluorodeoxyglucose uptake by proliferating and prenecrotic cancer cells in vivo: a microautoradiographic study. *J Nucl Med* 1994;35:1067–1075.
49. Higashi K, Clavo AC, Wahl RL. Does FDG uptake measure proliferative activity of human cancer cells? In vitro comparison with DNA flow cytometry and tritiated thymidine uptake. *J Nucl Med* 1993;34:414–419.

Technetium-99m-Labeled Anti-EGF-Receptor Antibody in Patients with Tumor of Epithelial Origin: I. Biodistribution and Dosimetry for Radioimmunotherapy

Normando Iznaga-Escobar, Leonel A. Torres, Alejo Morales, Mayra Ramos, Ivette Alvarez, Niuvis Pérez, Roberto Fraxedas, Oscar Rodríguez, Nelson Rodríguez, Rolando Pérez, Agustín Lage and Michael G. Stabin
Centers of Molecular Immunology, Clinical Research and Medical-Surgical Research, Institute of Nephrology, Orthopedic Hospital Frank País, Havana, Cuba; and Radiation Internal Dose Information Center, Oak Ridge, Tennessee

Accurate estimation of biodistribution and absorbed dose to normal organs and tumors is important for immunoscintigraphic studies and radioimmunotherapy treatment planning. **Methods:** Four patients (3 men, 1 woman; mean age 54.8 ± 9.2 yr; range 42–64 yr) were administered 3 mg of anti-human epidermal growth factor receptor (anti-hEGF-r) antibody (ior egf/r3), radiolabeled with ^{99m}Tc activity of 39.5 ± 1.1 mCi (range 38.5 mCi–40.7 mCi) by intravenous bolus infusion. After administration, blood and urine samples were collected from three patients up to 24 hr after injection. Whole-body anterior and posterior scans were obtained at 5 min and 1, 3, 5 and 24 hr after injection. Using a computer program, regions of interest were drawn over the heart, liver, spleen, bladder and tumor to measure the activity in the source organs at each scanning time. Time-activity curves for each source organ were then fitted to monoexponential or biexponential functions by nonlinear least squares regression using the flexible polyhedrals method, which adequately fit our data with the correlation coefficient of 0.985 ± 0.013, and were integrated to determine organ residence times. The mean absorbed doses to the whole body and various normal organs were then estimated from residence times and from blood and urine samples using the methods developed by the Medical Internal Radiation Dose Committee. The effective dose equivalent and effective dose were calculated as prescribed in ICRP Publication Nos. 30 and 60. **Results:** Plasma disappearance curves of ^{99m}Tc-labeled anti-hEGF-r antibody were best-fit by a two-compartment model in all patients with a distribution half-life ($t_{1/2\alpha}$) of 0.207 hr ± 0.059 hr (mean ± s.d., n = 3) and an elimination half-life ($t_{1/2\beta}$) of 13.9 hr ± 2.2 hr. Among the various organs, significant accumulation of the radiolabeled antibody was found in the liver (48.5% ± 4.4%, mean ± s.d.), heart (3.50% ± 0.17%) and spleen (3.1% ± 1.8%) at 5 min postadministration. These values were reduced to 3.2% ± 0.4%, 0.1% ± 0.01% and 0.1% ± 0.1%, respectively, at 24 hr. Mean cumulative urinary excretion of ^{99m}Tc-labeled anti-hEGF-r antibody was 4.6% ± 0.6% at 24 hr postinjection. Estimates of radiation absorbed dose to normal organs in rad/mCi administered (mean ± s.d., n = 4) were: whole body 0.017 ± 0.002; gallbladder wall 0.074 ± 0.007; spleen 0.136 ± 0.076; and liver 0.267 ± 0.036. The effective dose equivalent and effective dose estimates for adults were 0.041 ± 0.008 rem/mCi and 0.027 ± 0.004 rem/mCi administered. **Conclusion:** This feasibility study indicates that ^{99m}Tc-labeled anti-hEGF-r antibody (ior egf/r3) can be used safely; this analysis provides a dosimetric framework for future studies. This monoclonal antibody, labeled with ^{188}Re, could possibly permit a successful regional radioimmunotherapy of tumors of epithelial origin.

Key Words: biodistribution; dosimetry; radioimmunotherapy; human epidermal growth factor

J Nucl Med 1998; 39:15–23

The technique for the production of monoclonal antibodies (MAbs) of predefined specificity (*1*) resulted in a dramatic increase in the application of radiolabeled antibodies for radioimmunodiagnosis (RAID) and radioimmunotherapy (RAIT). Numerous clinical trials using radiolabeled MAbs for tumor detection, biodistribution and internal radiation dosimetry have been conducted in recent years (*2–4*). Significant positive results have now been achieved in RAID (*5,6*) and RAIT (*7–11*).

The calculation of the absorbed dose has been important in nuclear medicine. Such dose estimates are used to determine the health risks involved and the amount of radionuclides that should be administered to patients during routine procedures. The current Medical Internal Radiation Dose (MIRD) formalism (*12,13*) for estimating doses to individual organs usually includes the assumption of uniform radionuclide distribution in homogeneous media. Although this assumption is not strictly valid in many cases, its use in evaluating internal dose estimates for safety purposes remains routine.

The antibody ior egf/r3, developed at the Center of Molecular

Received Oct. 22, 1996; revision accepted Mar. 19, 1997.
For correspondence or reprints contact: Normando Iznaga-Escobar, Center of Molecular Immunology, P.O. Box 16040, Havana, 11600, Cuba.

TABLE 1
Patient Demographic Data

Patient no.	Age (yr)	Sex	Race	Weight (kg)	Height (cm)	Surface area (m^2)*	Plasma volume (ml)†	Diagnosis
6	42	F	W	52.0	154.0	1.49	2072	Lung cancer, Stage III
7	64	M	W	58.5	163.5	1.63	2572	Lung cancer, Stage IIIB
8	56	M	B	62.0	167.0	1.70	2678	Lung cancer
9	57	M	W	84.5	174.0	1.99	3140	Lung neoplasm with hepatomegaly
Mean ± s.d.	54.8 ± 9.2	—	—	64.3 ± 14.1	164.6 ± 8.3	1.70 ± 0.21	2615 ± 439	—

*Body surface area was calculated according to Ref. *24*.
†Total plasma volume was calculated according to Equation 1.
F = female; M = male; W = white; B = black.

Immunology (Havana, Cuba), is a murine IgG_{2a} MAb that binds to the external domain of the human epidermal growth factor receptor (hEGF-r). After binding to the receptor, the MAb-receptor complex is rapidly internalized, and a fraction of the MAb can be found in the nucleus of the cells. Because hEGF-r overexpression has been implicated in some human malignancies, such as gliomas (*14*) and breast (*15,16*), bladder (*17*), colon (*18*) and lung (*6,19*) tumors, MAbs against it have been used successfully during last years in the radioimmunodetection of these tumors.

In this article, we have evaluated the biodistribution, pharmacokinetics and internal radiation dosimetry to normal organs of the ^{99m}Tc-labeled MAb anti-hEGF-r (ior egf/r3) in patients with tumors of epithelial origin. A prediction of ^{188}Re dosimetry to normal organs and tumors for future RAIT has been made based on prior ^{99m}Tc imaging.

MATERIALS AND METHODS

Patients

Four patients with tumors of epithelial origin were selected from the Center for Medical-Surgical Research (Havana, Cuba) Phase I/II protocols. The study was approved by the Ethics Committee of the Center for Medical-Surgical Research Hospital and the National Regulatory Authorities of Cuba (Center for State Control of Quality of Drugs, Havana, Cuba). Technetium-99m-labeled MAb ior egf/r3 was administered to four patients (1 woman, 3 men; age range 42–64 yr; mean age 54.8 ± 9.2 yr) for biodistribution and internal radiation dosimetry studies. Table 1 provides demographic information on the patients, body surface area and total plasma volume. Written informed consent was obtained from all patients entered in the study.

Monoclonal Antibody

The MAb ior-egf/r3 is a highly specific murine IgG_{2a} isotype antibody that recognizes hEGF-r. The MAb ior egf/r3 is secreted by hybridoma A24/15/128, obtained by fusion of murine myeloma cells SP2/Ag14 with splenocytes from Balb/c mice, immunized with a partially purified fraction of the hEGF-r from human placental tissue. Its generation, characterization and reactivities have been described in detail elsewhere (*20,21*). Vials containing 1 ml of sterile and apyrogenic neutral solution with an antibody concentration of 5 mg/ml were used.

Radiolabeling and Quality Control

The ability of the reduced MAb to be labeled with ^{99m}Tc was assessed as previously described by Iznaga-Escobar et al. (*22*). Briefly, aliquots of 3 mg/ml reduced antibody were used. After reduction of intrinsic disulfide bonds, the Amerscan Medronate II bone-scanning kit (Amersham, London, UK) was reconstituted with 5 ml of 0.9% sodium chloride, purged with nitrogen. Antibody (50 μl/mg solution) was added to the reduced MAb and was labeled with 50 mCi of pertechnetate (TcO_4^-), eluted from a ^{99}Mo/^{99m}Tc generator. Activity was measured in a calibration system Compucal II (Nuclear Associates, Division of Victoreen, London, UK).

The labeled MAbs were analyzed by ascending chromatography on Whatman 3MM paper using 0.9% saline and methyl ethyl ketone (MEK) as a mobile phase. Strips (1 × 10 cm) were spotted with 1 μl of sample and eluted with either MEK or 0.9% saline for approximately 9 cm, dried and cut into three parts, two parts for MEK and one for saline. All parts were counted in a gamma counter (Scaler Ratemeter SR8; Nuclear Enterprise, London, UK) to quantitate the amount of protein-bound, non-protein-bound (^{99m}Tc-methylene diphosphonate) and free ^{99m}Tc activity.

Radiopharmaceutical Administration

Four patients were administered 39.5 mCi ± 1.1 mCi (mean ± s.d.; 3 mg of MAb) by intravenous bolus infusion through a peripheral vein. The appropriate dose was measured using a radioactivity calibration system (Compucal II). No adverse reactions were noticed in any of the patients during or after the infusion.

Blood and Urine Collection

After intravenous injection, 3–4 ml of blood samples were collected in three patients from the antecubital vein opposite of the injection side at timed intervals (2, 5, 10, 20 and 30 min and 1, 3, 5, 8, 18 and 24 hr postinjection). Samples of 1-ml aliquots of whole anticoagulated blood with heparin were immediately centrifuged (5 min at 3000 rpm) at room temperature, and plasma was removed with an Eppendorf pipette.

Urine was collected from each patient in 3-hr intervals for up to 24 hr, and the total volume of each collection was recorded.

The radioactivity in plasma and urine (0.3-ml aliquots) samples was determined in duplicate by counting in a fixed, reproducible geometry system gamma counter to obtain the total counts. All samples were counted for 10 sec, which generally provided a counting error of less than 1%, except for those from the later collection periods that contained low levels of radioactivity. The total counts in plasma and urine samples were then converted to activity concentration in μCi/ml using a standard prepared at the same time of the injection. Appropriate corrections were made for decay, using the time of injection as reference time.

Pharmacokinetic Data Analysis

For pharmacokinetic analysis, total plasma volume for each patient (Table 1) was obtained as previously described (*23*) using Equation 1. The obtained values were:

Males: TPV (in ml) = 1578 × S; and

Females: TPV (in ml) = 1395 × S, Eq. 1

where S is the body surface area in m^2, determined according to a previously described procedure (*24*). The plasma activity concentration in μCi/ml was multiplied by the total plasma volume to obtain whole plasma activity. Thereafter, plasma activity was expressed as the fraction of administered activity remaining in plasma at each counting time and related to the total injected dose (ID).

Plasma disappearance curves were fitted to a biexponential equation using a software package (BRASIER; provided by the High Institute of Nuclear Sciences and Technology, Havana, Cuba) which performs a nonlinear least squares regression analysis using the method of flexible polyhedrals (*25*). The selection of the two-compartment model over the others was performed according to the Akaike's information criteria (*26*) as a statistical test.

The plasma half-lives ($t_{1/2\alpha}$ and $t_{1/2\beta}$), the area under the time-activity curve and the maximal activity concentration (C_o) were calculated according to previously described methods (*27*). The apparent volume of the central compartment (V_c), apparent volume of distribution at steady state (V_{ss}) and plasma clearance (CL_D) were calculated according to standard methods (*28*).

Patient Imaging

Whole-body scans were performed on a Sophy DS-7 (Sopha Medical Systems, Ottawa, Canada) gamma camera, fitted with a low-energy, high-resolution, diverging parallel-hole collimator to increase the lateral viewing aspect. Images were acquired using a 20% window centered on the 140-keV emission from ^{99m}Tc after injection. Anterior and posterior whole-body scans were acquired at 5 min and 1, 3, 5 and 24 hr postinjection using a gantry speed of 20 cm/min; acquisition times were around 25 min each. All whole-body images were stored on the computer in a 2048 × 512 word mode matrix.

Biodistribution and Dosimetry Studies

Biodistribution studies were performed from whole-body anterior and posterior views taken at 5 min and 1, 3, 5 and 24 hr after injection. The geometric mean of anterior and posterior images corrected for decay was obtained using the computer program (BioDose, Version 1.0, Center for Clinical Research, Havana, Cuba). Using this program, regions of interest (ROIs) were drawn over heart, liver, spleen, bladder and tumor, which were the organs that took up enough radioactivity to be visualized on the images and which, therefore, were considered source organs. The geometric mean counts for source organs at each time interval were measured. Then the program converted total counts into activity and calculated the absolute activity concentration in μCi for each region of interest (ROI) at all imaging times. Accumulation of ^{99m}Tc-labeled MAb ior egf/r3 in nontarget organs was assessed from the ROIs. The geometric mean of the first whole-body anterior and posterior views was taken to represent 100% of the administered activity, and all the source organ and whole-body geometric means obtained from subsequent sessions were related to this value. Whole-body and source organ retention, in %ID, were expressed as the fraction of administered activity remaining in each source organ at each counting time and related to the geometric mean activity of the total body.

The source organs' time-activity data were then fit to either a monoexponential or biexponential function by a nonlinear least squares regression, using the flexible polyhedrals method, and were then integrated to obtain the cumulative activities to facilitate the calculation of residence times (*29*) for dosimetry purposes. The mean absorbed dose in mGy/MBq or rad/mCi to the total body and various target organs was then obtained using the residence times and the S values from (*30,31*) according to MIRD schema (*12,13*), with correction for the remainder of the body activity (*29*).

The urinary bladder time-activity curves were typically sawtooth-shaped curves and were fitted using a dynamic bladder model. The cumulative activity A_R (AUC) was obtained by integrating from zero to the last void point of the equation that describes a sawtooth-shaped curve and divided by the ID to obtain bladder residence time. The radiation absorbed dose to the bladder was then calculated based on the effective mean residence time for the ^{99m}Tc-labeled MAb ior egf/r3 in the bladder, which was derived from the bladder time-activity curves. The amount of radioactivity excreted from the ID and then corrected for radioactive decay was obtained by measurement of the radioactivity contained in urine collections over a specific time interval. One practical difficulty in determining mean residence time by this method is the need to collect multiple complete urine collections for as long as possible after injection of the radiopharmaceutical.

The effective dose equivalent and effective dose were calculated from the mean values of 24 normal organ absorbed doses according to the methods given in ICRP Publication Nos. 30 and 60 (*32,33*).

Predicting Dose for Normal Organs

The prediction of absorbed doses to normal organs for ^{188}Re-RAIT from prior ^{99m}Tc-labeled MAb ior egf/r3 imaging was performed by calculation of the effective half-times in each source organ from the ^{99m}Tc activity curves and assuming the biodistributions of ^{99m}Tc- and ^{188}Re-labeled MAb ior egf/r3 to be similar. The effective half-time for the ^{188}Re immunoconjugates was estimated from Equation 2:

$$1/T_e\ (^{188}Re) = 1/T_b\ (^{99m}Tc) + 1/T_p\ (^{188}Re), \qquad \text{Eq. 2}$$

where T_b = biological half-time, T_e = effective half-time and T_p = physical half-time of the radioisotope. The calculated values for the effective half-time of ^{188}Re in each source organ were used to predict the absorbed dose to normal organs.

Tumor Dosimetry

Tumor dosimetry was more difficult to estimate when there was a low concentration of activity in the tumor compared with the surrounding background activity. The content of radioactivity in the tumor from the time of injection up to 24 hr postinjection was used to develop tumor time-activity curves of ^{99m}Tc-labeled MAb ior egf/r3 in two patients. The integral of tumor activity was computed trapezoidally by assuming activity equals zero at time zero, and then tumor residence times were obtained, from which absorbed doses were estimated using the MIRD formalism (*12,13*).

Calculation of tumor dosimetry for RAIT was based on the biological half-life of the tumor (11.90 hr) for ^{99m}Tc-labeled MAb ior egf/r3 and the physical half-life of ^{188}Re (16.9 hr), to develop an effective half-life of 19.63 hr. With tumor residence times and based on an absorbed dose constant S-factor of 6.73×10^{-1} rad/μCi · hr (for ^{188}Re), the absorbed dose was calculated. The absorbed dose to tumor as was estimated, included the total dose from nonpenetrating radiation (from radioactivity concentrated in the tumor) and penetrating radiation from gamma rays emitted by radioactivity in the source organs. The gamma contributions were dependent on the location and position of the tumor in relationship to the source organs.

Statistical Analysis

Data were analyzed to give mean and s.d. values. Statistical significance of differences between patients were determined by the software MicroCal Origin Version 3.0 (MicroCal Software, Inc., Northampton, MA) using paired two-tailed Student's t-test when appropriate, with $p < 0.05$ being considered significant.

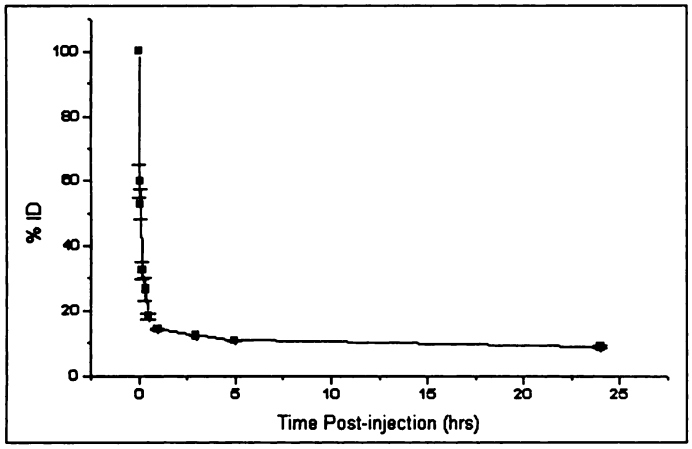

FIGURE 1. Plasma clearance curve after ^{99m}Tc-labeled MAb ior egf/r3 intravenous bolus injection in three patients entered in this study. Values plotted represent the mean for three individuals. There were no statistically significant differences between individuals ($p < 0.05$).

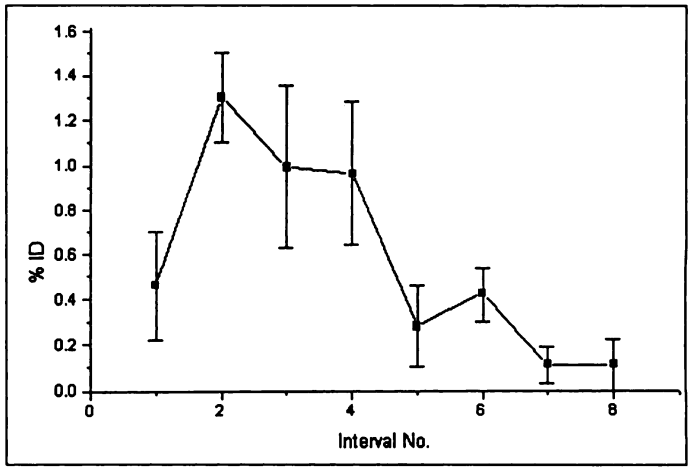

FIGURE 2. Urinary excretion pattern of ^{99m}Tc-labeled MAb ior egf/r3 in 3-hr intervals up to 24 hr postinjection. Values represent the mean and s.d. for three individuals. The urinary excretion patterns were essentially identical for all individuals.

RESULTS

Biodistribution Studies

Biodistribution studies were conducted to quantify immunospecific localization and to provide a basis for developing dose estimates. The mean plasma clearance curve of the ^{99m}Tc-labeled MAb ior egf/r3 is shown in Figure 1. The best fit plasma time-activity curves in all patients had a distribution half-life ($t_{1/2\alpha}$) of 0.207 ± 0.059 hr (mean ± s.d., n = 3) and an elimination half-life ($t_{1/2\beta}$) of 13.9 ± 2.2 hr (Table 2). The statistical differences between patients were calculated by two-tailed paired Student's t-test. The AUC was 25.2 ± 13.7 (μCi/ml · hr) and the C_o was 8.5 ± 1.5 μCi/ml. The mean apparent volume of the central compartment was 76.9 ± 27.9 ml/kg, the mean apparent steady-state volume of distribution was 509.8 ± 352.5 ml/kg and the mean systemic clearance was 34.7 ± 27.3 ml/hr · kg.

Activity in the urine, when represented as %ID per 3-hr urine collection, was low (Fig. 2). In the three patients studied, a maximum occurred at 3–6 hr after injection. The mean %ID of ^{99m}Tc-labeled MAb ior egf/r3 excreted in the urine by 24 hr postinfusion under physiological conditions was 4.6% ± 0.6%. There were no significant differences between all patients at the $p < 0.05$ level for all pharmacokinetic parameters.

After administration of ^{99m}Tc-labeled MAb ior egf/r3, the liver, heart and spleen were evident immediately and were still visible through 24 hr postinjection (Fig. 3). The mean biological clearance curves for whole body, remainder of the body, liver, heart, spleen and urinary bladder obtained from gamma camera imaging for ^{99m}Tc in four patients are shown in Figure 4. There was insufficient radioactivity for kidneys and lungs to be considered as a source organs for dose estimates in all patients. The normal organ biodistribution and whole-body kinetics were calculated from whole-body anterior and posterior views taken at different time intervals. The uptakes in the most important source organs, liver, heart, spleen and urinary bladder, and the remainder of the body, were determined as a function of time. Radioactivity in the urinary bladder was calculated using the measured radioactivity excreted in the urine and assuming a bladder voiding interval of 3 hr (*32*). Radioactivity in the remainder of the body (expressed as percentage of the administered activity) as a function of time was determined as 100% minus the percentage uptake in liver, heart, spleen, urinary bladder and excreted radioactivity in urine. Time courses of radioactivity in the liver, heart and spleen showed close similarities between individual patients (data not shown). The results of the uptake measurements are given in Figure 4. Among the various organs significant accumulation of the radiolabeled was found in the liver (48.5% ± 4.4%, mean ± s.d.), heart (3.50% ± 0.17%), spleen (3.1% ± 1.8%) and bladder (0.53% ± 0.4%) at 5 min postadministration. These values were reduced to 3.2% ± 0.4%, 0.1% ± 0.01%, 0.1% ± 0.1% and 0.06% ± 0.03%, respectively, at 24 hr postinjection. Localization of the radioactivity in the liver after injection of ^{99m}Tc-labeled MAb ior egf/r3 was rapid, with great retention up to 5 hr postinjection because of the number of hEGF-r present in it (Fig. 4). The liver is the organ with the largest number of sites of excretion and/or metabolism of radiolabeled MAbs and their degradation products. Good clearance was seen from the liver, 3.2 %ID at 24 hr postinjection.

TABLE 2
Pharmacokinetic Parameters of Technetium-99m-Labeled MAb ior egf/r3 Intravenous Bolus Injection in Three Patients

Pharmacokinetic parameter	Mean (range)
$t_{1/2\alpha}$ (hr)	0.207 (0.139–0.246)
$t_{1/2\beta}$ (hr)	13.9 (12.6–16.4)
AUC (μCi/ml · hr)	25.2 (11.4–38.7)
C_o (μCi/ml)	8.5 (6.9–9.9)
V_c(ml/kg)	76.9 (54.6–168.2)
V_{SS}(ml/kg)	586.7 (211.6–970.3)
CL_D (ml/hr · kg)	34.7 (12.4–65.2)

AUC = cumulative activity; C_o = maximal activity concentration; V_c = apparent volume of the central compartment; V_{ss} = apparent volume of distribution at steady state; CL_D = plasma clearance.

Dosimetry Studies

Here, dose calculations for normal organs based on the MIRD formalism (*12,13*) for ^{99m}Tc-labeled MAb ior egf/r3 were performed in four patients using the residence times showed in Table 3. The uptake of radioactivity in the liver, heart, spleen and urinary bladder was measured with the gamma camera. Other organs (e.g., the kidneys and lungs) showed low accumulation of radioactivity and were disregarded in the gamma camera measurements. Instantaneous uptake, homogeneous distribution and monoexponential or biexponential clearance of the radioactive substance from the tissues was assumed. Radioactivity excreted in the urine was used for calculation of

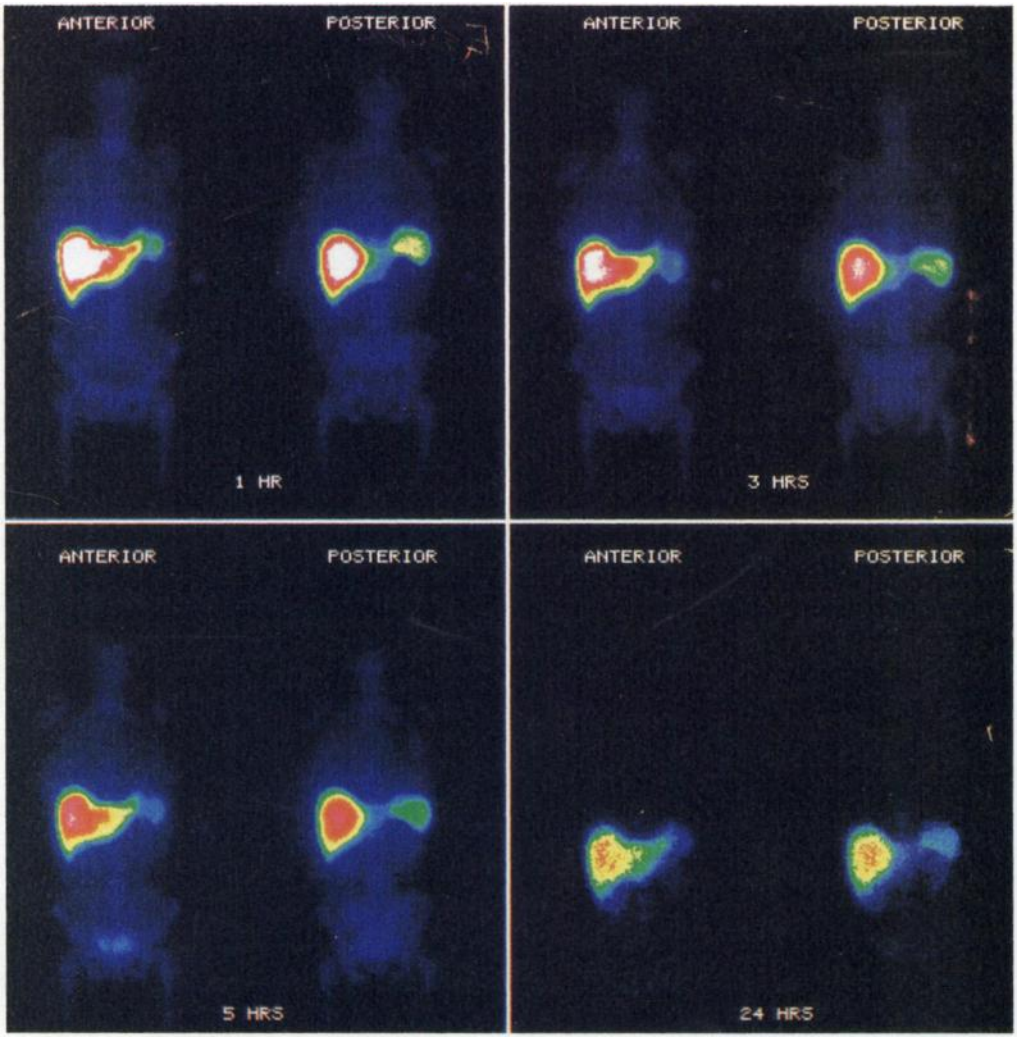

FIGURE 3. Serial whole-body anterior and posterior scans of ^{99m}Tc-labeled MAb ior egf/r3 in Patient 7, taken at 1, 3, 5 and 24 hr after injection, indicating early accumulation in liver and spleen.

the residence time of the urinary bladder contents for all patients and showed the same course as the mean depicted in Figure 2. Table 4 shows the average absorbed dose estimates to normal organs for a 3 mg (39.5 ± 1.1 mCi) dose of ^{99m}Tc-labeled MAb ior egf/r3, expressed as mGy/MBq or rad/mCi administered. Estimates of radiation absorbed dose to normal organs in rad/mCi administered (mean ± s.d., n = 4) were: whole body 0.017 ± 0.002; gallbladder wall 0.074 ± 0.007; spleen 0.136 ± 0.076; and liver 0.267 ± 0.036. The liver received the highest dose. The reason for the large accumulation of activity in liver and its retention was the high number of hEGF-r present in the hepatocytes, which leads to the antigen-antibody complex formation.

The effective dose equivalent and effective dose estimates shown in Table 5 for adults were 0.041 ± 0.008 rem/mCi and 0.027 ± 0.004 rem/mCi administered. There were no statistically significant differences in the dose estimates of the various normal organs or in the effective dose equivalent or effective dose in comparison to the direct estimates for each individual (data not shown).

Predicting Dose for Normal Organs

The mean absorbed doses to normal organs predicted for ^{188}Re-labeled MAb ior egf/r3, assuming the biodistribution of ^{99m}Tc-labeled MAb ior egf/r3 to be similar in the four patients, are shown in Table 6. In this table, the total absorbed dose in rad for a 50-mCi administration is included. Paired Student's t-test indicated no significant differences between individuals in predicted dosimetry for normal organs. Predicted values of radiation absorbed dose to normal organs in rad/mCi administered (mean ± s.d., n = 4) were: whole body 0.400 ± 0.012; urinary bladder wall 0.241 ± 0.018; heart wall 1.00 ± 0.18; spleen 9.61 ± 5.04; and liver 10.65 ± 0.17. The effective dose equivalent and effective dose predicted for ^{188}Re are shown in Table 6; for adults, they were 0.53 ± 0.16 rem/mCi and 0.34 ± 0.11 rem/mCi administered, respectively.

Tumor Dosimetry

Accurate ROIs were drawn in Patient 6, who had a primary lung cancer Stage III that had metastasized to the laryngeal region, and also in Patient 9, a 57-yr-old man with a primary lung neoplasm and hepatomegaly, who had a metastatic region with an area of increased ^{99m}Tc-labeled MAb ior egf/r3 activity in the right anterior pectoral area. The integral of the time-activity curve for the tumor (Fig. 5) was computed trapezoidally by assuming activity equals zero at time zero and the residence time was determined. Based on tumor residence time of 19.63 hr and the absorbed dose constant S for ^{188}Re, the absorbed dose was calculated. For the tumor, it was 19.92 ± 3.51 rad/mCi administered. Based on these results for two patients, it was assumed that the tumor uptake of the ^{188}Re-labeled MAb ior egf/r3 in these patients would be the same as that for the ^{99m}Tc-labeled MAb ior egf/r3. After injection of 150 mCi of ^{188}Re-labeled MAb ior egf/r3, the tumor would receive a total dose of about 3000 rad.

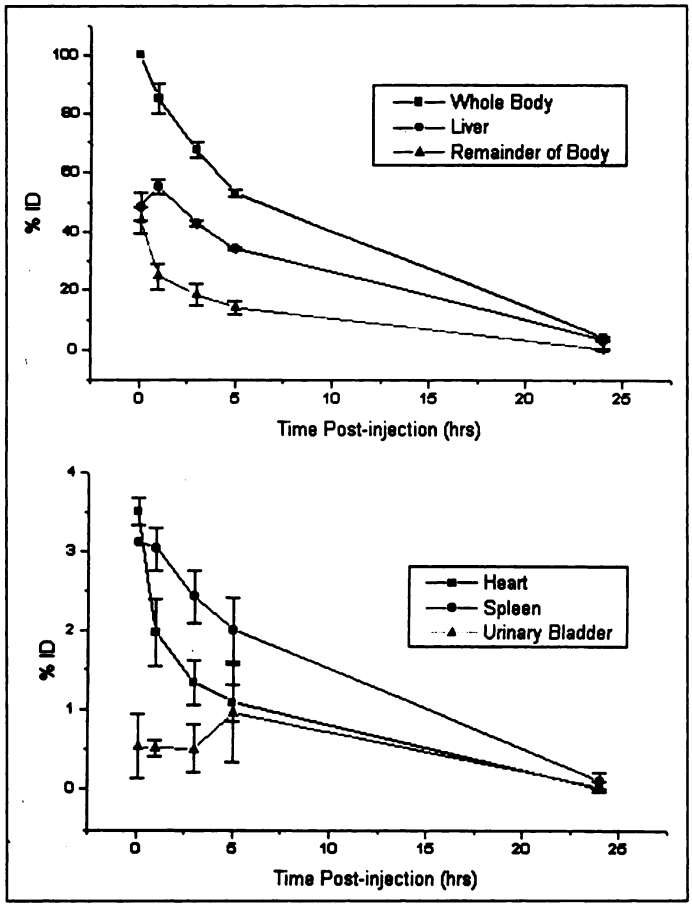

FIGURE 4. Normal organ biodistribution and whole-body kinetics of ^{99m}Tc-labeled MAb ior egf/r3 administered in a 3-mg dose by intravenous bolus injection, as determined by whole-body scans in a gamma camera and expressed as %ID.

DISCUSSION

The advances made in the development of anticancer MAbs and their successful use in diverse laboratory and clinical procedures have spurred considerable interest in their potential role in the diagnosis and treatment of cancer (*11*). At present, a small number of antibodies exist that have been produced specifically against hEGF-r (*6,34–38*). Of these, few have properties that are compatible with RAID (*6,38*) and RAIT (*34,39*).

The physical properties of ^{99m}Tc allow good-quality images to be acquired on a gamma camera for assessing radiopharmaceutical biodistribution, and this permitted the use of relatively simple procedures to make the quantification of activity from gamma camera images and derive dosimetry estimates. The resolution of the images was such that ROIs could be drawn on source organs without requiring administration of additional radionuclides to define organ boundaries (*40*) or blood-pool scans for background subtraction (*41*).

TABLE 3
Source Organ Residence Times

Source organs	Residence time (hr)	
	^{99m}Tc	^{188}Re
Heart contents	0.183 ± 0.0338	0.51 ± 0.09
Liver	5.74 ± 0.13	12.13 ± 0.22
Spleen	0.383 ± 0.205	1.05 ± 0.55
Urinary bladder contents	0.050 ± 0.00408	0.048 ± 0.004
Remainder of body	1.49 ± 0.36	3.85 ± 0.87

Development of accurate methods to determine absorbed dose is important so that the tolerance of the normal tissues to low-dose radiation can be better defined. Once this is known, RAIT could be planned to deliver the highest doses to the tumors.

The quality control studies showed good incorporation of ^{99m}Tc onto the MAb, excellent immunoreactivity assessed by a radio receptor assay (*42*) and good stability of the ^{99m}Tc-labeled MAb ior egf/r3 in vivo, with only a small amount of ^{99m}Tc transcomplexed from the MAb to plasma proteins (*27*).

The MAb ior egf/r3, a murine IgG_{2a} isotype, was cleared from the circulation of the patients with biexponential kinetics consisting of an initial or alpha phase, with a half-life of about 0.207 hr ± 0.059 hr, representing in part the distribution of the antibody between the vascular and extravascular compartments, and a second or beta phase of 13.9 hr ± 2.2 hr, representing the catabolism of antibody fully equilibrated between the two compartments. The half-lives obtained in our studies are also consistent with previous clearance studies with other murine MAbs conducted over a comparable time scale, which measured half-lives between 0.1 hr and 24 hr (*43*).

We examined the biodistribution from quantification of activity on the gamma camera images, estimated internal radiation doses to normal organs and made a prediction of ^{188}Re dosimetry from a prior ^{99m}Tc imaging. Time-activity curves for each source organ were fitted to monoexponential or biexponential functions by nonlinear least squares regression, using the flexible polyhedrals method, which adequately fit our data with the correlation coefficient of 0.985 ± 0.013, and were integrated to determine organ residence times. The absorbed doses to the whole body and to normal organs were estimated using the residence times and the standard MIRD male/female anthropomorphic models. Radioactivity excreted in the urine was used for calculation of the residence time of the urinary bladder contents for all patients and showed the same course as the mean depicted in Figure 2.

It was difficult to obtain accurate quantification of activity in tumors within normal organs because of varying background activities, particularly in lung lesions, where fluid and atelectasis could not be distinguished from tumor and where activity was not high enough relative to background activity to draw accurate ROIs for Patients 7 and 8. We could draw ROIs in Patient 6, who had a primary lung cancer Stage III that had metastasized to the laryngeal region, and also in Patient 9, a 57-yr-old man with a primary lung neoplasm and hepatomegaly, who had a metastatic region with an area of increased ^{99m}Tc-labeled MAb ior egf/r3 activity in the right anterior pectoral area. Absorbed doses to tumor tissues for ^{188}Re were estimated using the same approach as taken for normal organs (*44,45*). Tumors were modeled as normal organs of similar mass and position in the body.

The majority of literature references quote a possible 1000- to 2000-rad radiation dose to typical tumors studied, depending on isotope used, antibody biodistribution and number of administrations (*46,47*). The absorbed radiation doses calculated by the method described in this article for normal organs are in general agreement with the estimates of dose to tumor and normal organ reported by others in a series of patients treated with ^{131}I- and ^{186}Re-labeled antitumor antibodies (*9,48*). Dose estimates in these studies for the whole body are 10 and 4 times higher than that of ^{188}Re-labeled MAb ior egf/r3, respectively, although predicted dose to the liver and tumor were similar. In our study, the liver absorbed dose estimates are relatively high, due to the number of hEGF-r present. Student's t-test indicated no significant differences between dose to the liver and tumor in our

TABLE 4
Normal Organ Dosimetry for Technetium-99m-Labeled MAb ior egf/r3 (mean ± s.d.)

Target organ	mGy/MBq*	rad/mCi*
Adrenals	$1.12 \times 10^{-2} \pm 1.32 \times 10^{-3}$	$4.16 \times 10^{-2} \pm 4.86 \times 10^{-3}$
Brain	$7.40 \times 10^{-4} \pm 1.34 \times 10^{-4}$	$2.74 \times 10^{-3} \pm 4.97 \times 10^{-4}$
Breast	$2.32 \times 10^{-3} \pm 2.56 \times 10^{-4}$	$8.59 \times 10^{-3} \pm 9.51 \times 10^{-4}$
Gallbladder wall	$1.99 \times 10^{-2} \pm 1.85 \times 10^{-3}$	$7.38 \times 10^{-2} \pm 6.86 \times 10^{-3}$
LLI wall	$1.53 \times 10^{-3} \pm 1.84 \times 10^{-4}$	$5.66 \times 10^{-3} \pm 6.69 \times 10^{-4}$
Small intestine	$3.79 \times 10^{-3} \pm 4.07 \times 10^{-4}$	$1.40 \times 10^{-2} \pm 1.51 \times 10^{-3}$
Stomach	$5.53 \times 10^{-3} \pm 1.16 \times 10^{-3}$	$2.05 \times 10^{-2} \pm 4.28 \times 10^{-3}$
ULI wall	$5.32 \times 10^{-3} \pm 5.96 \times 10^{-4}$	$1.97 \times 10^{-2} \pm 2.23 \times 10^{-3}$
Heart wall	$1.00 \times 10^{-2} \pm 1.04 \times 10^{-3}$	$3.25 \times 10^{-2} \pm 9.90 \times 10^{-3}$
Kidneys	$8.22 \times 10^{-3} \pm 1.02 \times 10^{-3}$	$3.27 \times 10^{-2} \pm 4.59 \times 10^{-3}$
Liver	$7.21 \times 10^{-2} \pm 9.71 \times 10^{-3}$	$2.67 \times 10^{-1} \pm 3.58 \times 10^{-2}$
Lungs	$6.03 \times 10^{-3} \pm 8.80 \times 10^{-4}$	$2.23 \times 10^{-2} \pm 3.27 \times 10^{-3}$
Muscle	$2.65 \times 10^{-3} \pm 2.86 \times 10^{-4}$	$9.80 \times 10^{-3} \pm 1.04 \times 10^{-3}$
Ovaries	$2.08 \times 10^{-3} \pm 2.32 \times 10^{-4}$	$7.68 \times 10^{-3} \pm 8.58 \times 10^{-4}$
Pancreas	$1.16 \times 10^{-2} \pm 2.00 \times 10^{-3}$	$4.27 \times 10^{-2} \pm 7.33 \times 10^{-3}$
Red marrow	$2.81 \times 10^{-3} \pm 2.07 \times 10^{-4}$	$1.04 \times 10^{-2} \pm 7.70 \times 10^{-4}$
Bone surfaces	$4.52 \times 10^{-3} \pm 4.81 \times 10^{-4}$	$1.67 \times 10^{-2} \pm 1.77 \times 10^{-3}$
Skin	$1.41 \times 10^{-3} \pm 1.19 \times 10^{-4}$	$5.19 \times 10^{-3} \pm 4.46 \times 10^{-4}$
Spleen	$3.68 \times 10^{-2} \pm 2.06 \times 10^{-2}$	$1.36 \times 10^{-1} \pm 7.62 \times 10^{-2}$
Testes	$8.74 \times 10^{-4} \pm 1.63 \times 10^{-4}$	$3.24 \times 10^{-3} \pm 6.06 \times 10^{-4}$
Thymus	$2.77 \times 10^{-3} \pm 2.67 \times 10^{-4}$	$1.03 \times 10^{-2} \pm 9.93 \times 10^{-4}$
Thyroid	$1.08 \times 10^{-3} \pm 1.68 \times 10^{-4}$	$4.00 \times 10^{-3} \pm 5.97 \times 10^{-4}$
Urinary bladder wall	$3.38 \times 10^{-3} \pm 6.32 \times 10^{-4}$	$1.25 \times 10^{-2} \pm 2.31 \times 10^{-3}$
Uterus	$2.07 \times 10^{-3} \pm 2.20 \times 10^{-4}$	$7.64 \times 10^{-3} \pm 8.17 \times 10^{-4}$
Total body	$4.66 \times 10^{-3} \pm 5.25 \times 10^{-4}$	$1.73 \times 10^{-2} \pm 1.90 \times 10^{-3}$

*There were no statistical differences between all patients ($p < 0.05$ by paired Student's t-test). LLI = lower large intestine; ULI = upper large intestine.

subjects for the predicted dosimetry of ^{131}I-, ^{186}Re- and ^{188}Re-labeled antibodies. The estimated dose to whole body for ^{131}I-, ^{186}Re- and ^{188}Re-labeled antitumor antibodies studies were different because the contribution of the penetrating and nonpenetrating radiation to a mass centrally located in the body varied for ^{131}I, ^{186}Re and ^{188}Re (Δ_i values are approximately 0.40, 0.76 and 1.70 g · rad/μCi · hr, respectively, for these three nuclides).

Using the methods described, the calculations given here appear to be generally valid for calculation of normal tissue dosimetry after RAIT with ^{188}Re immunoconjugates. For RAIT, it appears that 2000–2500 rad delivered by an isotope conjugated to an antitumor MAb may be sufficient to result in a radiation-mediated tumor response. On the basis of dosimetry calculations, we predict that the dose to the individual tumors will be between 2500 rad and 3000 rad after the injection of 150 mCi of ^{188}Re-labeled MAb ior egf/r3. Animal models have shown that doses to tumor of 2000–3000 rad can cure nude mice of small (18 mm^3) tumors (*49*).

The theoretical advantages of radioimmunoscintigraphy are clear. For the first time, we have available a diagnostic reagent that is specifically directed at tumors and is not dependent on nonspecific findings, such as ultrasound reflection, paramagnetic properties, mass effect or attenuation characteristics. As more clinical sites embark on therapeutic trials, methods to quantitate the activity must be as practical and reproducible as possible so that data can be compared among the various radioimmunoconjugates and that the most appropriate therapy will be selected for patients. The dosimetry formalism presented above may facilitate calculation of more accurate doses and establishment of meaningful dose-response relationships for experimental radionuclide therapy. The excellent labeling methods that have now been developed for ^{99m}Tc and ^{188}Re (*50*), the availability of generators for both radionuclides and the possibility of having a freeze-dried kit formulation have made suggested that ^{99m}Tc and ^{188}Re may constitute an ideal "matched pair" radionuclide combination for imaging, patient selection and RAIT, making the use of ^{99m}Tc- and ^{188}Re-labeled antibodies feasible for research and clinical applications.

CONCLUSION

This study was undertaken to evaluate the biodistribution, estimate the internal radiation absorbed dose to normal organs of ^{99m}Tc-labeled MAb ior egf/r3 and make a prediction of absorbed dose to normal organs and tumor of ^{188}Re-labeled MAb ior egf/r3 based on prior ^{99m}Tc imaging. This feasibility study indicates that ^{99m}Tc-labeled anti-hEGF-r antibody (ior egf/r3) can be used safely, and that adequate doses can be administered for diagnostic imaging without exposing the patient to excessive radiation. Thus, this provides a dosimetric framework for future studies. We believe that this study has

TABLE 5
Effective Dose Equivalent and Effective Dose Estimates for Adults

	^{99m}Tc		^{188}Re	
	mSv/MBq	rem/mCi	mSv/MBq	rem/mCi
Effective dose equivalent	$1.12 \times 10^{-2} \pm 2.09 \times 10^{-3}$	$4.14 \times 10^{-2} \pm 7.80 \times 10^{-3}$	$3.70 \times 10^{-1} \pm 7.28 \times 10^{-2}$	$1.37 \times 10^{-0} \pm 2.70 \times 10^{-1}$
Effective dose	$7.17 \times 10^{-3} \pm 9.95 \times 10^{-4}$	$2.65 \times 10^{-2} \pm 3.68 \times 10^{-3}$	$2.35 \times 10^{-1} \pm 4.70 \times 10^{-2}$	$8.76 \times 10^{-1} \pm 1.72 \times 10^{-1}$

TABLE 6
Normal Organ Dosimetry Predicted for Rhenium-188-Labeled MAb ior egf/r3 (mean ± s.d., 3 mg of MAb, 50 mCi)

Target organ	mGy/MBq*	rad/mCi*	Total rad
Adrenals	$3.40 \times 10^{-2} \pm 5.41 \times 10^{-3}$	$1.26 \times 10^{-1} \pm 2.01 \times 10^{-2}$	6.300
Brain	$2.49 \times 10^{-2} \pm 5.62 \times 10^{-3}$	$9.24 \times 10^{-2} \pm 2.09 \times 10^{-2}$	4.618
Breast	$2.64 \times 10^{-2} \pm 5.59 \times 10^{-3}$	$9.77 \times 10^{-2} \pm 2.05 \times 10^{-2}$	4.885
Gallbladder wall	$4.13 \times 10^{-2} \pm 5.74 \times 10^{-3}$	$1.52 \times 10^{-1} \pm 2.13 \times 10^{-2}$	7.575
LLI wall	$2.56 \times 10^{-2} \pm 5.64 \times 10^{-3}$	$9.49 \times 10^{-2} \pm 2.08 \times 10^{-2}$	4.745
Small intestine	$2.75 \times 10^{-2} \pm 5.59 \times 10^{-3}$	$1.02 \times 10^{-1} \pm 2.05 \times 10^{-2}$	5.085
Stomach	$2.91 \times 10^{-2} \pm 5.07 \times 10^{-3}$	$1.08 \times 10^{-1} \pm 1.78 \times 10^{-2}$	5.389
ULI wall	$2.88 \times 10^{-2} \pm 5.59 \times 10^{-3}$	$1.07 \times 10^{-1} \pm 2.06 \times 10^{-2}$	5.328
Heart wall	$2.73 \times 10^{-1} \pm 4.88 \times 10^{-2}$	$1.00 \times 10^{-0} \pm 1.78 \times 10^{-1}$	50.30
Kidneys	$3.16 \times 10^{-2} \pm 5.15 \times 10^{-3}$	$1.17 \times 10^{-1} \pm 1.91 \times 10^{-2}$	5.846
Liver	2.88 ± 0.05	10.65 ± 0.17	532.5
Lungs	$2.93 \times 10^{-2} \pm 5.56 \times 10^{-3}$	$1.08 \times 10^{-1} \pm 2.08 \times 10^{-2}$	5.421
Muscle	$2.66 \times 10^{-2} \pm 5.53 \times 10^{-3}$	$9.86 \times 10^{-2} \pm 2.06 \times 10^{-2}$	4.930
Ovaries	$2.61 \times 10^{-2} \pm 5.62 \times 10^{-3}$	$9.65 \times 10^{-2} \pm 2.08 \times 10^{-2}$	4.823
Pancreas	$3.41 \times 10^{-2} \pm 4.73 \times 10^{-3}$	$1.26 \times 10^{-1} \pm 1.76 \times 10^{-2}$	6.313
Red marrow	$2.69 \times 10^{-2} \pm 5.55 \times 10^{-3}$	$9.95 \times 10^{-2} \pm 2.07 \times 10^{-2}$	4.976
Bone surfaces	$2.74 \times 10^{-2} \pm 5.66 \times 10^{-3}$	$1.01 \times 10^{-1} \pm 2.09 \times 10^{-2}$	5.066
Skin	$2.56 \times 10^{-2} \pm 5.53 \times 10^{-3}$	$9.47 \times 10^{-2} \pm 2.05 \times 10^{-2}$	4.735
Spleen	2.60 ± 1.36	9.61 ± 5.04	480.6
Testes	$2.51 \times 10^{-2} \pm 5.58 \times 10^{-3}$	$9.26 \times 10^{-2} \pm 2.07 \times 10^{-2}$	4.628
Thymus	$2.69 \times 10^{-2} \pm 5.73 \times 10^{-3}$	$9.96 \times 10^{-2} \pm 2.11 \times 10^{-2}$	4.979
Thyroid	$2.53 \times 10^{-2} \pm 5.62 \times 10^{-3}$	$9.35 \times 10^{-2} \pm 2.07 \times 10^{-2}$	4.675
Urinary bladder wall	$6.51 \times 10^{-2} \pm 5.06 \times 10^{-3}$	$2.41 \times 10^{-1} \pm 1.85 \times 10^{-2}$	12.03
Uterus	$2.61 \times 10^{-2} \pm 5.68 \times 10^{-3}$	$6.12 \times 10^{-2} \pm 4.02 \times 10^{-2}$	3.059
Total body	$1.08 \times 10^{-1} \pm 3.16 \times 10^{-3}$	$4.00 \times 10^{-1} \pm 1.20 \times 10^{-2}$	20.00

*There were no statistical differences between all patients ($p < 0.05$ by paired Student's t-test). LLI = lower large intestine; ULI = upper large intestine.

important implications for future clinical trials involving radioimmunodetection and that this MAb, labeled with ^{188}Re, could possible permit a successful regional RAIT of tumors of epithelial origin.

ACKNOWLEDGMENTS

We thank Jorge A. Carrasquillo, MD, from the Department of Nuclear Medicine (National Cancer Institute, National Institutes of Health, Bethesda, MD) for his expertise in reviewing the manuscript. We are grateful to the Center of Clinical Researches (Havana, Cuba), the Department of Nuclear Medicine of the Orthopedic Hospital Frank País and the Department of Nuclear Medicine of the Center for Medical-Surgical Research (Havana, Cuba) for their technical assistance and for excellent support of the study.

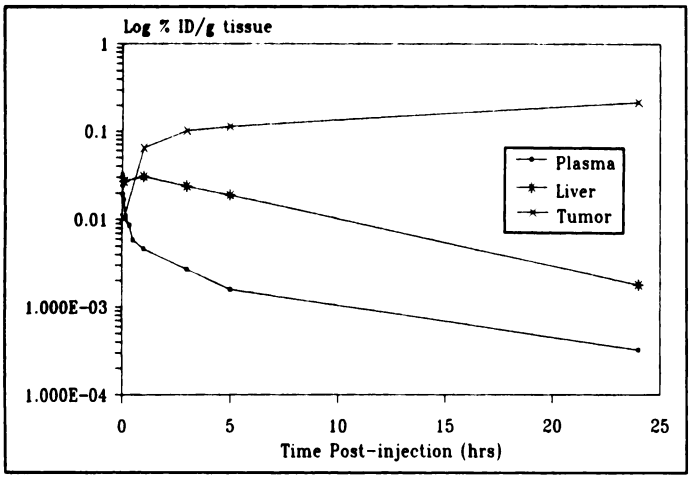

FIGURE 5. Tumor and liver uptake kinetics and plasma clearance curve of ^{99m}Tc-labeled MAb ior egf/r3 administered in a 3-mg dose by intravenous bolus injection, as determined by whole-body scans in a gamma camera and blood measurements and expressed as log (%ID/g) of tissue. Tumor = 2 g; liver = 1800 g; plasma = 3100 g.

REFERENCES

1. Kohler G, Milstein C. Continuous cultures of fused cells secreting antibody of predefined specificity. *Nature* 1975;256:495–499.
2. Breitz HB, Durham JS, Fisher DR, et al. Pharmacokinetics and normal organ dosimetry following intraperitoneal rhenium-186-labeled monoclonal antibodies. *J Nucl Med* 1995;36:754–761.
3. Noz ME, Kramer EL, Maguire GQ Jr, McGee SA, Sanger JJ. An integrated approach to biodistribution radiation absorbed dose estimates. *Eur J Nucl Med* 1993;20:165–169.
4. Maraveyas A, Stafford N, Rowlinson-Busza G, Stewart JSW, Epenetos AA. Pharmacokinetics, biodistribution, and dosimetry of specific and control radiolabeled monoclonal antibody in patients with primary head and neck squamous cell carcinoma. *Cancer Res* 1995;55:1060–1067.
5. Reilly RM. Immunoscintigraphy of tumors using ^{99m}Tc-labeled monoclonal antibodies: a review. *Nucl Med Commun* 1993;14:347–359.
6. Divgi CR, Welt S, Kris M, et al. Phase I and imaging trial of indium 111-labeled anti-epidermal growth factor receptor monoclonal antibody 225 in patients with squamous cell lung carcinoma. *J Natl Cancer Inst* 1991;83:97–104.
7. Schroff RW, Weiden PL, Appelbaum J, et al. Rhenium-186 labeled antibody in patients with cancer: report of a pilot Phase I study. *Antibody Immunoconj Radiopharm* 1990;3:99–111.
8. Breitz HB, Weiden PL, Vanderheyden JL, et al. Clinical experience with rhenium-186-labeled monoclonal antibodies for radioimmunotherapy: results of Phase I trials. *J Nucl Med* 1992;33:1099–1112.
9. Breitz HB, Fisher DR, Weiden PL, et al. Dosimetry of rhenium-186-labeled monoclonal antibodies: methods, prediction from technetium-99m-labeled antibodies and results of Phase I trials. *J Nucl Med* 1993;34:908–917.
10. Jacobs AJ, Fer M, Min Su F, et al. A Phase I trial of a rhenium-186-labeled monoclonal antibody administered intraperitoneally in ovarian carcinoma: toxicity and clinical response. *Obstet Gynecol* 1993;82:586–593.
11. Goldenberg DM, Griffiths GL. Radioimmunotherapy of cancer: arming the missiles. *J Nucl Med* 1992;33:1110–1112.
12. Loevinger R, Berman M. A revised schema for calculating the absorbed dose from biologically distributed radionuclides. In: *A revised schema for calculating the absorbed dose from biologically distributed radionuclides*, MIRD Pamphlet No. 1, revised. New York: Society of Nuclear Medicine; 1976:7–14.
13. Loevinger R, Budinger TF, Watson EE. *MIRD primer for absorbed dose calculations*. New York: Society of Nuclear Medicine; 1988:1–14.
14. Snelling L, Miyamoto CT, Bender H, et al. Epidermal growth factor receptor 425 monoclonal antibodies radiolabeled with iodine-125 in the adjuvant treatment of high-grade astrocytomas. *Hybridoma* 1995;14:111–114.
15. Pérez R, Pascual MR, Macias A, Lage A. Epidermal growth factor receptors in human breast cancer. *Breast Cancer Res Treat* 1984;4:189–193.

16. Rios MA, Fernández A, Tormo BR, et al. Heterogenous expression of the EGF receptor in human breast carcinoma. *Anticancer Res* 1992;12:205–208.
17. Neal DE, March C, Benett MK, et al. Epidermal growth factor receptors in human bladder cancer. Comparison of invasive and superficial tumors. *Lancet* 1985;i:346–348.
18. Magnusson I, Rosen AV, Nilsson R, Macias A, Pérez R, Skoog L. Receptors for epidermal growth factor and sex steroid hormones in human colorectal carcinomas. *Anticancer Res* 1989;9:299–302.
19. Veale D, Ashcroft T, March C, Gibson GJ, Harris AL. Epidermal growth factor receptors in non-small cell lung cancer. *Br J Cancer* 1987;55:513–516.
20. Fernández A, Pérez R, Macias A, et al. Generación y caracterización primaria de anticuerpos monoclonales contra el receptor del factor de crecimiento epidérmico. *Interferón Biotecnol* 1989;6:289–299.
21. Fernández A, Spitzer E, Pérez R, et al. A new monoclonal antibody for detection of EGF-receptors in Western blots and paraffin-embedded tissue sections. *J Cell Biochem* 1992;49:157–165.
22. Iznaga-Escobar N, Morales A, Núñez G. Micromethod for quantification of SH groups generated after reduction of monoclonal antibodies. *J Nucl Med Biol* 1996;23:641–644.
23. Pearson TC, Guthrie DL, Simpson J, et al. Interpretation of measured red cell mass and plasma volume in adults. *Br J Haematol* 1995;89:748–756.
24. Dubois D, Dubois EF. A formula to estimate the approximate surface area if height and weight be known. *Arch Intern Med* 1916;17:863–871.
25. Jennrich RI, Sampson PF. Application of stepwise regression to nonlinear least squares estimation. *Techometrics* 1968;10:63–72.
26. Akaike A. Posterior probabilities for choosing regression model. *Ann Inst Math Stat* 1978;30:A9–A14.
27. Iznaga-Escobar N, Torres LA, Morales A, et al. Technetium-99m-labeled anti-EGF-receptor antibody in patients with tumor of epithelial origin. II. Pharmacokinetics and clearances. *J Nucl Med* 1998;39:in press.
28. Gibaldi M, Perrier D. Pharmacokinetics. In: Gibaldi M, Perrier D, eds. *Pharmacokinetics*, 2nd Ed. New York: Marcel Dekker Inc.; 1982:319–355.
29. Stabin MG. Patient dose from diagnostic and therapeutic radiopharmaceuticals. In: Raabe OG, ed. *Internal radiation dosimetry: Health Physics Society 1994 Summer School*. Madison, WI: Medical Physics Publishing; 1995:375–392.
30. Snyder WS, Ford MR, Warmer GG, Watson SB. *"S" absorbed dose per unit cumulated activity for selected radionuclides and organs*, MIRD Pamphlet No. 11. New York: Society of Nuclear Medicine; 1975.
31. Snyder WS, Ford MR, Warmer GG, Fisher HL. Estimates of absorbed fractions for monoenergetic photon sources uniformly distributed in various organs of a heterogeneous phantom. In: *Medical internal radiation dose (MIRD)*, Vol. 5. New York: Society of Nuclear Medicine; 1978:50–67.
32. International Commission on Radiological Protection (ICRP). *Limits for intakes of radionuclides by workers*, ICRP Publ. No. 30. New York: Pergamon Press; 1979:1–13.
33. International Commission on Radiological Protection (ICRP). *Recommendations of the International Commission on Radiological Protection*, ICRP Publ. No. 60. New York: Pergamon Press; 1991;21:1–3.
34. Baselga J, Mendelsohn J. The epidermal growth factor receptor as a target for therapy in breast carcinoma. *Breast Cancer Res Treat* 1994;29:127–138.
35. Khetarpal VK, Storbeck LS. Biological disposition of intravenously administered ^{131}I-labeled anti-EGF-receptor antibody (RG 83852) in rat. *Cancer Chemother Pharmacol* 1995;35:313–317.
36. Murthy U, Basu A, Rodeck U, Herlyn M, Ross AH, Das M. Binding of antagonistic monoclonal antibody to an intact and fragmented EGF-receptor polypeptide. *Arch Biochem Biophys* 1987;72:77–89.
37. Takahashi H, Nakazawa S, Herlyn D. Experimental radioimmunotherapy of a xenografted human glioma using ^{131}I-labeled monoclonal antibody to epidermal growth factor receptor. *Neurol Med Chir Tokyo* 1993;33:610–615.
38. Dadparvar S, Krishna L, Miyamoto C, et al. Indium-111-labeled anti-EGFr-425 scintigraphy in the detection of malignant gliomas. *Cancer* 1994;73(suppl):884–889.
39. Steiner K, Haunschild J, Faro HP, Senekowitsh R. Distribution of humanized MAb 425 (EMD 62 000) in rats and specific localization in tumor-bearing nude mice. *Cell Mol Biol* 1995;41:179–184.
40. Hammond ND, Moldofsky PJ, Bearsley MR, et al. External imaging techniques for quantitation of distribution of ^{131}I-labeled F(ab')$_2$ fragments of monoclonal antibody in humans. *Med Phys* 1984;11:778–783.
41. Eary JF, Appelbaum FL, Durack L, et al. Preliminary validation of the opposing view method for quantitative gamma camera imaging. *Med Phys* 1989;16:382–387.
42. Macias A, Pérez R, Lage A. Estudios sobre el factor de crecimiento epidérmico. II. Desarrollo de un radio-receptor análisis para la determinación de cantidades picomolares. *Interferón Biotecnol* 1985;2:115–127.
43. Kirkwood JM, Neumann RD, Zoghbi SS, et al. Scintigraphic detection of metastatic melanoma using indium-111/DTPA conjugated anti-gp240 antibody (ZME-018). *J Clin Oncol* 1987;5:1247–1255.
44. Wessels B, Rogus RD. Radionuclide selection and model absorbed dose calculations for radiolabeled tumor associated antibodies. *Med Phys* 1984;11:638–675.
45. Fisher DR, Badger CC, Breitz HB, et al. Internal radiation dosimetry for clinical testing of radiolabeled monoclonal antibodies. *Antibody Immunoconj Radiopharm* 1991;4:655–664.
46. Epenetos AA, Snook D, Durbin H, Johnson PM, Taylor-Papadimitriou J. Limitations of radiolabeled monoclonal antibodies for localization of human neoplasms. *Cancer Res* 1986;46:3183–3191.
47. Dykes PW, Bradwell AR, Chapman CE, Vaughan ATM. Radioimmunotherapy of cancer: clinical studies and limiting factors. *Cancer Treat Rev* 1987;14:87–106.
48. Leichner PK, Klein JL, Garrison JB, et al. Dosimetry of ^{131}I-labeled anti-ferritin in hepatoma: a model for radioimmunoglobulin dosimetry. *Int J Radiat Oncol Biol Phys* 1981;7:323–333.
49. Beaumier PC, Venkatesan P, Vanderheyden JL, et al. Re-186 radioimmunotherapy of small cell lung carcinoma xenografts in nude mice. *Cancer Res* 1991;51:676–681.
50. Griffiths GL, Goldenberg DM, Knapp FF Jr, et al. Direct radiolabeling of monoclonal antibodies with generator-produced rhenium-188 for radioimmunotherapy: labeling and animal biodistribution studies. *Cancer Res* 1991;51:4594–4602.

Diagnosis of Recurrent Glioma with SPECT and Iodine-123-α-Methyl Tyrosine

Torsten Kuwert, Burkhard Woesler, Carlo Morgenroth, Hartmut Lerch, Michael Schäfers, Stefan Palkovic, Peter Matheja, Wolfgang Brandau, Hansdetlef Wassmann and Otmar Schober

Departments of Nuclear Medicine and Neurosurgery, Westfälische Wilhelms-Universität, Münster, Germany

Iodine-123-α-methyl tyrosine (IMT) allows the investigation of amino acid transport rate in brain neoplasms. It was the aim of this study to evaluate the potential of IMT-SPECT to diagnose the recurrence of gliomas after primary therapy. **Methods:** Using a triple-headed SPECT camera, the cerebral uptake of IMT was determined in 27 patients 22 mo, on average, after surgical removal of a primary brain tumor. Eighteen patients had suffered from high-grade gliomas, and nine had suffered from low-grade tumors. Four patients were examined before and after surgical revision of a presumed tumor recurrence. A total of 31 studies were evaluated. The final diagnosis was based on prospective clinicopathological follow-up. Recurrence was diagnosed in 23 cases, with marked clinical deterioration occurring 3.1 mo, on average, after SPECT, and was confirmed by histopathology in 14 instances. Eight cases were free of recurrence, as evidenced by inconspicuous clinical follow-up, ranging from 6 mo to 17 mo after SPECT in seven cases, and by clinical course and histopathology in the remaining subject. **Results:** Patients with recurrence had significantly higher ratios of IMT uptake in the tumor area to that in a background region than did patients without recurrence (2.27 ± 0.59 compared to 1.47 ± 0.29; $p < 0.002$). The best cutoff level of the IMT uptake ratio in the differentiation between recurrence and benign posttherapeutic lesion was 1.8. Using this study-specific discrimination threshold, the sensitivity and specificity of IMT-SPECT for detecting glioma recurrence were 18 of 23 (78%) and 8 of 8 (100%), respectively. The area under the binormal receiver operating characteristic curve, fitted to the data, was 0.90 ± 0.06. **Conclusion:** Iodine-123-α-methyl tyrosine-SPECT is a promising new tool in the follow-up of patients with gliomas after primary therapy.

Key Words: SPECT; iodine-123-α-methyl tyrosine; amino acids; brain neoplasms; gliomas

J Nucl Med 1998; 39:23–27

Received Oct. 28, 1996; revision accepted Mar. 14, 1997.

For correspondence or reprints contact: Torsten Kuwert, MD, Department of Nuclear Medicine, Westfälische Wilhelms-Universität Münster, Albert-Schweitzer-Strasse 33, 48129 Münster, Germany.